Local density functional calculations of the electronic structures of Ti_2AlC and Ti_3AlC

Samir F. Matar, Yann Le Petitcorps and Jean Etourneau

Institut de Chimie de la Matière Condensée de Bordeaux–CNRS, Château Brivazac, Avenue du Docteur Schweitzer, F33600 Pessac, France

Local density functional calculations are used to address the electronic structures and the properties of chemical bonding of two definite phases formed within the ternary system Ti, Al and C: Ti_2AlC and Ti_3AlC. From the analyses of the density of states and of the crystal orbital overlap populations of the respective phases within the ASW method the role of C is assessed. Moreover, the bonding within TiC is discussed concomitantly. These calculations are of interest in the composite field to understand the mechanisms of formation of new compounds at the matrix/reinforcement interface.

Carbon fibre-reinforced titanium–aluminium intermetallic composite materials are of interest for space and aeronautics applications. In recent years several works have been devoted to their investigation, both experimentally[1–3] and theoretically.[4,5,6] From the latter point of view, we modelled recently the influence of substituted and inserted carbon within the alloy lattice of TiAl on its electronic structure.[6] Based on quantitatively resolved chemical bonding criteria we proposed that carbon should substitute preferentially for aluminium when it enters the TiAl lattice. This is supported by the actual occurrence of Ti-rich carbide compounds such as Ti_2AlC in the immediate neighbourhood of the intermetallic matrix of TiAl. Moreover, the growth of such a carbide phase from this alloy leads to an enrichment of Al atoms at the intermetallic/ternary compound interface. For the titanium-rich alloy Ti_3Al, carbon is inserted to give Ti_3AlC. In all cases TiC is formed in the vicinity of the carbon fibre (Fig. 1). Thus Ti–C interactions form TiC, whereas Ti_2AlC and Ti_3AlC are formed respectively with the TiAl–C and Ti_3Al–C couples, according to a diffusion path determined by Clochefert.[3]

In this, the second part of our investigation of carbon-containing TiAl, we address the electronic properties of the titanium-rich carbides Ti_2AlC and Ti_3AlC actually forming in the {Ti–Al–C} phase diagram, with the objective of examining the influence of carbon on the chemical bonding within the alloy lattice.

Method of calculation

As in our earlier investigation,[6] the electronic properties of all carbon-containing alloy systems were calculated using the *ab initio* self-consistent augmented spherical wave (ASW) method.[7] The ASW method allows one to describe the electronic properties of a material starting from those of its atomic constituents. The calculations are based on the density functional theory in which the effects of exchange and correlation are treated in the local density approximation within the scheme of von Barth and Hedin, and Janak.[8] The ASW method uses the atomic sphere approximation (ASA) where each atom is surrounded by a sphere. Within the atomic spheres the potential is assumed to be spherically symmetric. The ASA imposes a unit-cell volume equal to the total volume of the spheres, leading to their overlap. This is unproblematic for close-packed crystal structures, but for loosely packed ones the empty space must be represented by use of 'empty spheres' (ES), *i.e.*, pseudo-atoms with $Z=0$ atomic number and no core states. ES are introduced in order to account for the interstitial space in the lattice and to avoid the use of otherwise unreasonably large atomic sphere radii leading to a large overlap in the ASA.

In *k*-space, the Brillouin zone integration is achieved on a uniform mesh of points in the irreducible wedge of the relevant Bravais lattice. The matrix elements are constructed involving solutions of the Schrödinger equation up to the secondary l quantum number, $l_{max}+1$, where $l_{max}=2$ for Ti and Al and 1 for C and the ES. The contributions associated with the $l_{max}+1$ higher angular momenta are relative to non-explicitly calculated terms in the limited ASW basis set[7] but should always be lower than 0.1 electron in order to ensure a convergence of

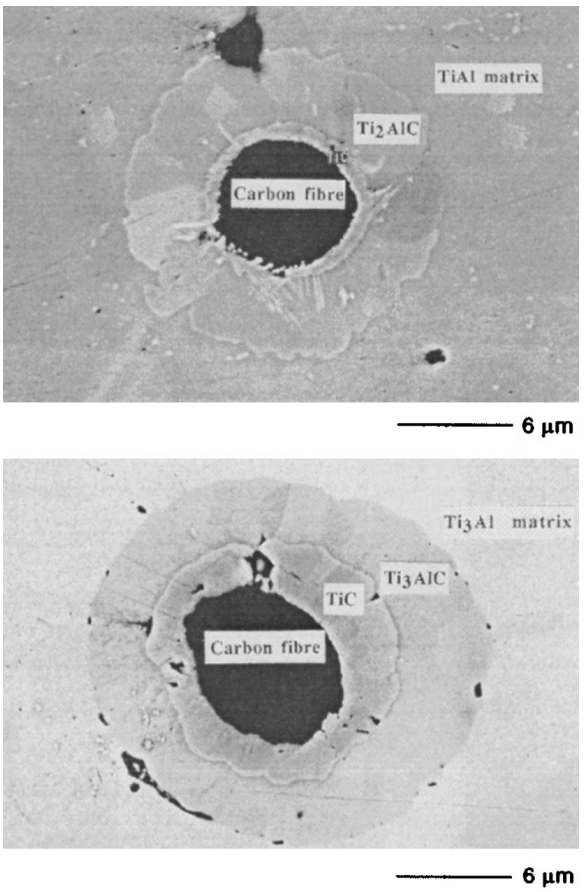

Fig. 1 Electron micrographs of the chemical interaction between carbon and Ti–Al intermetallics. Upper: C–TiAl; lower: C–Ti_3Al. (Reproduced with permission from ref. 3.)

the charges. The self-consistent cycle is carried out until the following convergence criteria are reached: $\Delta E = 10^{-8}$ Ry [1 Ry (rydberg) = 13.6 eV] for the total energy and $\Delta Q = 10^{-8}$ for the charge difference between two successive cycles. In this work all calculations were carried out at the experimental lattice constants obtained from ref. 3. Furthermore, in this work the chemical bonding features are discussed based on the so-called COOP (read CO-OP: crystal orbital overlap populations), of which a comprehensive account was given by Hoffmann from the quantum chemistry standpoint (extended Hückel calculations).[9] This allows for the DOS features to be discussed on bases of chemical bonding criteria by weighting them with the sign and magnitude of the overlap integral between the relevant orbitals. We recently implemented the COOP in the ASW method[10] with the objective of obtaining more precise information on the chemical bonding from first principles.

Crystal structures and setup of the unit cells for ASW calculations

In contrast to several Ti_2AlM (M = Nb, V, Cr, Mn) compounds which crystallize in a tetragonal structure,[5] Ti_2AlC is hexagonal with a large *c* axis and two formula units per cell. It crystallizes in the Cr_2AlC-type structure[11] with the $P6_3/mmc$ space group and Ti at (4f), Al at (2c) and C at (2a) Wyckoff positions. The structure is shown in Fig. 2(*a*). It can be regarded as an alternating stacking of triangular prisms and octahedral Ti polyhedra containing Al and C atoms, respectively, along the *c*-axis. Ti_6C octahedra share edges and form two-dimensional layers perpendicular to the *c* axis. From this low dimensionality, the structure is poorly packed and in the ASA, ES had to be introduced between the layers at sites related to those of Ti general positions.

With one formula unit per unit cell, Ti_3AlC has a structure derived from the cubic perovskite ABX_3 (where A and B are large and small cations at corner and centre positions, and X is an anion at face centres of the cube; space group $Pm3m$). Therefore Ti_3AlC [Fig. 1(*b*)] can be described as an antiperovskite because Ti atoms occupy the face centres, Al and C being at corner and cube-centre positions respectively. From the point of view of coordination polyhedra, the structure can be regarded as a three-dimensional array of Ti_6C octahedra sharing corners. It is hence a poorly packed structure because the midpoints of the edges, $\frac{1}{2}$ 0 0, 0 $\frac{1}{2}$ 0 and 0 0 $\frac{1}{2}$, are vacant sites where ES had to be introduced in the ASA.

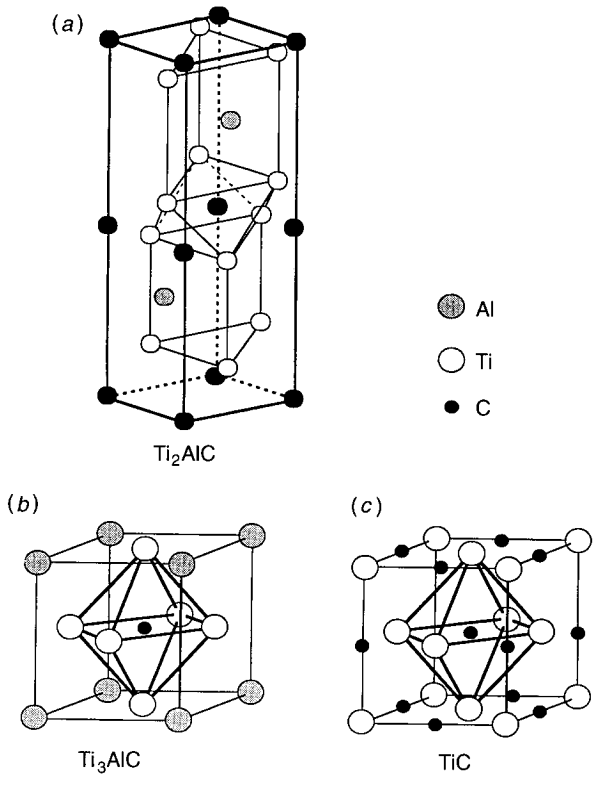

Fig. 2 (*a*) Hexagonal structure of Ti_2AlC. (*b*) Perovskite-derived structure of Ti_3AlC. (*c*) NaCl-type structure of TiC. (Reproduced with permission from ref. 3.)

Before examining the electronic structures of these two carbides, it is relevant to consider the coordination polyhedra in TiC. We stress that this binary carbide is modelled here in a 1:1 composition although it is known to be sub-stoichiometric in carbon, *i.e.* TiC_x with $0.56 < x < 0.98$.

TiC crystallizes in the NaCl-type structure (space group $Fm3m$) with four formula units per unit cell [Fig. 2(*c*)]. Ti and C are at the origin and $\frac{1}{2}$ $\frac{1}{2}$ $\frac{1}{2}$ positions, respectively. Ti and C are octahedrally coordinated with each other; consequently, Ti_6C octahedra share edges.

By comparing the three structures an interesting observation appears: dimensionality increases from Ti_2AlC to Ti_3AlC and TiC.

Ad hoc and non-unique choices of the atomic spheres radii in the ASA were such that: $r_{Ti}/r_{ES} = 1.26$, $r_{Al}/r_{ES} = 1.30$ and $r_C/r_{ES} = 1.10$. Such values were tested as one choice which simultaneously minimizes the overlap between the spheres and yields in converged $l_{max}+1$ residual charges.

Calculations and Results

Partial charges

Table 1 gives the partial charges for Ti_2AlC and Ti_3AlC (ΔQ designates the deviation from neutrality). The overall features of charge transfer are similar, in that it occurs from the two metallic atoms towards the non-metal and the empty spheres, *i.e.* Ti,Al→C,ES. The average departure from neutrality per metal is then *ca.* 0.73 in Ti_2AlC and *ca.* 0.79 in Ti_3AlC. In as far as carbon receives *ca.* 0.6 electrons in both carbides, this charge excess leads to the larger occupancy of ES in the latter. However, the differences which characterize the ΔQ values of Ti and Al in each compound should be addressed. They arise from the fact that Al exhibits a larger d character in Ti_2AlC (represented by the higher d occupancy) than in Ti_3AlC. This should indicate a larger hybridization between Ti and Al in Ti_2AlC with respect to Ti_3AlC. By virtue of this mixing there is an enhancement of the sp character of Ti which could be due to its interaction with Al and/or with C. This establishes a covalent character of the bonding in these materials, to be further illustrated in next section.

Density of states (DOS)

The upper panels (*a*) of Fig. 3 and 4 show the site-projected DOS of Ti_2AlC and Ti_3AlC. Energy reference along the *x* axis

Table 1 Site and *l*-projected partial charges for Ti_2AlC and Ti_3AlC

	s	p	d	f	ΔQ
$Ti_2AlC(ES)_2$:[a]					
Al	1.08	0.82	0.23	(0.02)	−0.84
Ti	0.37	0.56	2.33	(0.08)	−0.67
C	1.40	3.05	0.15	(0.02)	0.62
ES	0.54	0.20	(0.04)	—	0.78
$Ti_3AlC(ES)_3$:[b]					
Al	0.88	1.25	0.15	(0.01)	−0.69
Ti	0.32	0.51	2.28	(0.07)	−0.82
C	1.29	3.07	0.21	(0.03)	0.60
ES	0.62	0.19	(0.05)	—	0.85

[a] $Q = 2(-0.67) - 0.84 + 0.62 + 2(0.78) = 0$ (neutrality). [b] $Q = 3(-0.82) - 0.69 + 0.60 + 3(0.85) = 0$ (neutrality).

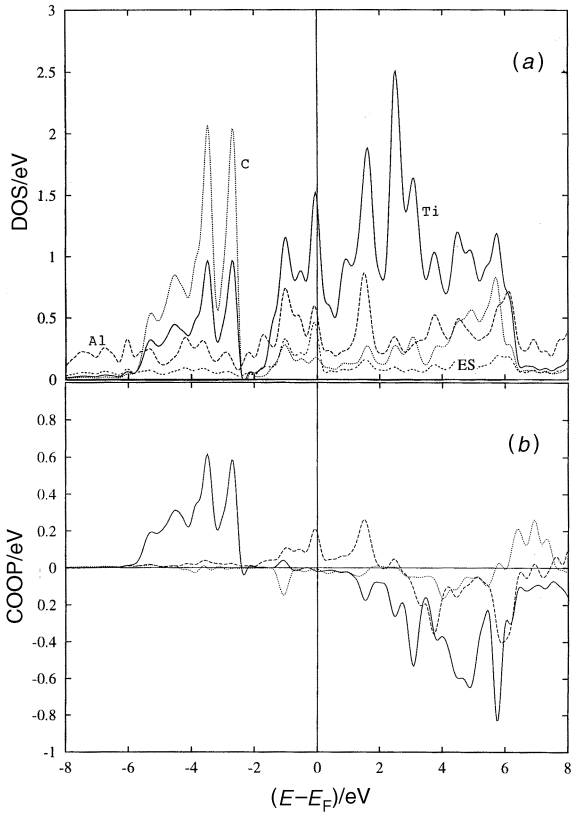

Fig. 3 Ti_2AlC: (*a*) site projected densities of states in $atom^{-1}\,eV^{-1}$ (solid line Ti; dashed line Al; dotted line C; dash-dotted line ES); (*b*) partial COOP for pair interactions: Ti–C (solid line), Ti–Al (dashed line), Al–C (dotted line)

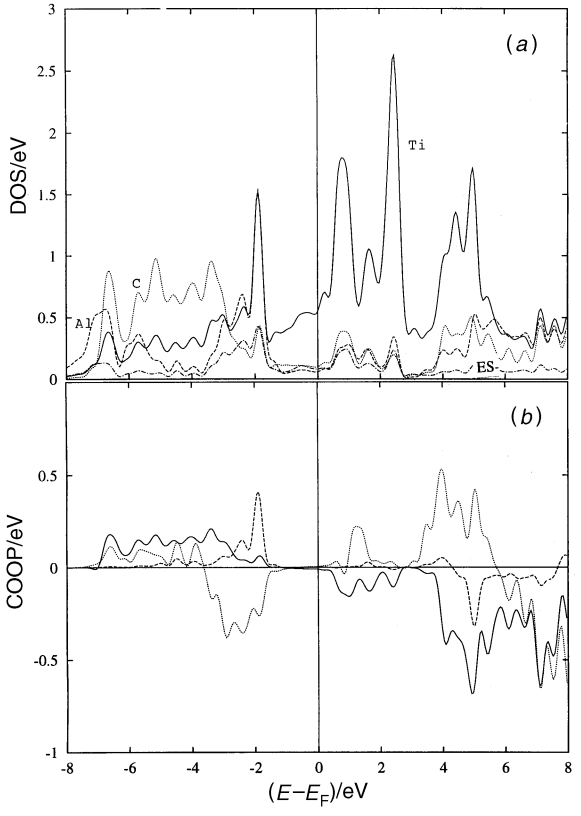

Fig. 4 Ti_3AlC: (*a*) site projected densities of states in $atom^{-1}\,eV^{-1}$ (solid line Ti; dashed line Al; dotted line C; dash-dotted line ES); (*b*) partial COOP for pair interactions: Ti–C (solid line), Ti–Al (dashed line), Al–C (dotted line)

is taken with respect to the Fermi level (E_F) within a reduced energy range (−8 to +8 eV), *i.e.* excluding the low lying C 2s states, to make the presentation clear. The *y* axis gives the DOS per atom and unit energy ($atom^{-1}\,eV^{-1}$). In both carbides, the Fermi level crosses the lower part of the Ti 3d states centred above E_F because of the nearly empty d band. These states show much larger structures towards the lower energies than in TiAl,[6] where they interact solely with Al s,p states because of the extra interaction with carbon. This is shown by the peaks between −6 and −4 eV in Ti_2AlC and −7 and −3 eV in Ti_3AlC. From a preliminary crystal-field analysis, the peaks in Ti DOS at −2, 1 and 2 eV arise mainly from in-plane *xy* and x^2-y^2 d orbitals. However, it is difficult to separate totally the contributions of the five different d orbitals because of their hybridization and of the collective character of the electrons. The DOS at E_F, $n(E_F)$, are dominated by Ti 3d and show a sharp peak in Ti_2AlC, probably due to Ti–C interactions (see next section) whereas such a feature is absent in Ti_3AlC where $n(E_F)$ are three times lower. There is a larger contribution from Al states at and above E_F in Ti_2AlC which agrees with our discussion of the charges, leading to a mixing between Ti 3d and Al 3p. In Ti_3AlC the DOS are dominated by carbon and Ti on one hand and Ti d on the other hand below and above E_F, respectively. Al plays a less important role at E_F in this carbide and its 'sp' DOS are seen in the energy windows −8 to −6 eV and −4 to −2 eV. A relevant feature is the broadness of the band over the energy range −8 to −2 eV as opposed to the sharp peaks in the same range in Ti_2AlC. In both compounds the DOS of the ES closely follow those of the other species, which is consistent with charge transfer into them from the other sites.

At this point the discussion of the mixing features solely from the partial DOS cannot give more information about the chemical bonding in the two compounds. A further step must be undertaken, by examining the COOP.

Crystal orbital overlap populations (COOP)

The features of chemical bonding can be assessed further by using the COOP. In the lower panels (*b*) of Fig. 3 and 4, the COOP are shown for the interactions between the different atoms in the two compounds plotted in the same energy range, *i.e.* for Ti–C, Ti–Al and Al–C. Along the *y*(COOP) axis, positive, negative and zero values point to bonding, antibonding and non-bonding states, respectively. In Ti_2AlC, below E_F, Ti–C interactions predominate, whereas in TiAl Ti–Al interactions are the driving interaction for the bonding.[6] They exhibit largely bonding character in the range −6 to −2 eV, and follow exactly the Ti DOS in the same energy range in which C 2p states dominate. Thus the sp character introduced into Ti (*cf.* Table 1) mainly arises from its interaction with carbon. The antibonding counterpart can be seen in the conduction band (2 to 6 eV). The large separation between the bonding and antibonding peaks is indicative of a strong interaction assimilated with a σ-like interaction. This somehow opposes the Ti–C interaction in Ti_3AlC, where less localized bonding states are seen to extend over a wide band in a larger energy window (σ- and π-like bonding). Interestingly, carbon is engaged not only in Ti–C interactions but also in Al–C ones, Ti–C and Al–C interactions having bonds in the same energy range. This is in contrast to Ti_2AlC, where only Ti–C interactions are present in the valence band. This is supported experimentally, whereby the solubility of carbon is much more important in Ti_3Al than in TiAl.[11] However, the Al–C bond seems weaker because it is largely antibonding from −4 to −2 eV whereas Ti–C is bonding over a wider energy range.

For the Ti–Al interaction, the distance between these two sites is 23% shorter in Ti_2AlC than in Ti_3AlC. This should explain the differences appearing between the two panels for the Ti–Al interaction and should assess the d character brought

into Al by its bonding with Ti (*cf.* Table 1). As a matter of fact, Ti–Al becomes important only around E_F, *i.e.* in the DOS region where Ti d states predominate. In contrast, Ti–Al interactions in Ti_3AlC are mainly seen in the energy range of Al 3p states, around -2 eV, in the same energy range as Ti–C and Al–C bonds with the largest bonding contribution at the top of the valence band, whereas they are nearly absent in the Ti–C energy range in Ti_2AlC owing to the nearly two-dimensional array of Ti_6C octahedra.

Comparison with TiC

At this point a comparison with the electronic structure of TiC is in order. Fig. 5(*a*) gives the site-projected DOS of TiC. They are in good agreement with those of Blaha and Schwarz (ref. 12 and refs. cited therein) who gave a full account of the electronic structures of TiX (X = C, N, O) compounds by use of a linearized APW (augmented plane waves) method. The feature of the $n(E_F)$ minima at the Fermi level is related to the refractory nature of TiX and their stability.[13] From -6 eV to E_F, C 2p states predominate, whereas from E_F to 8 eV, Ti 3d states with their t_{2g} ($\leqslant 4$ eV) and e_g (>4 eV) components show the major contribution to the DOS. In the valence band and from 4 eV to higher energies, C and Ti states have similar shapes, which is indicative of a covalent interaction between them. The DOS of ES follow the same evolution as the Ti and C ones, indicating that charge transfer into them is from both species.

In the purely O_h point symmetry, Ti 3d orbitals split into two types of manifold: t_{2g} and e_g. The projection of the DOS along them is shown in Fig. 6. In the valence band, e_g orbitals have a larger contribution with respect to t_{2g} ones; they are involved with pd_σ-type bonding with carbon whereas pd_π bonding should be less involved. Since metal Ti–Ti interactions are of the dd_σ type, one expects little bonding of this type in the valence band.

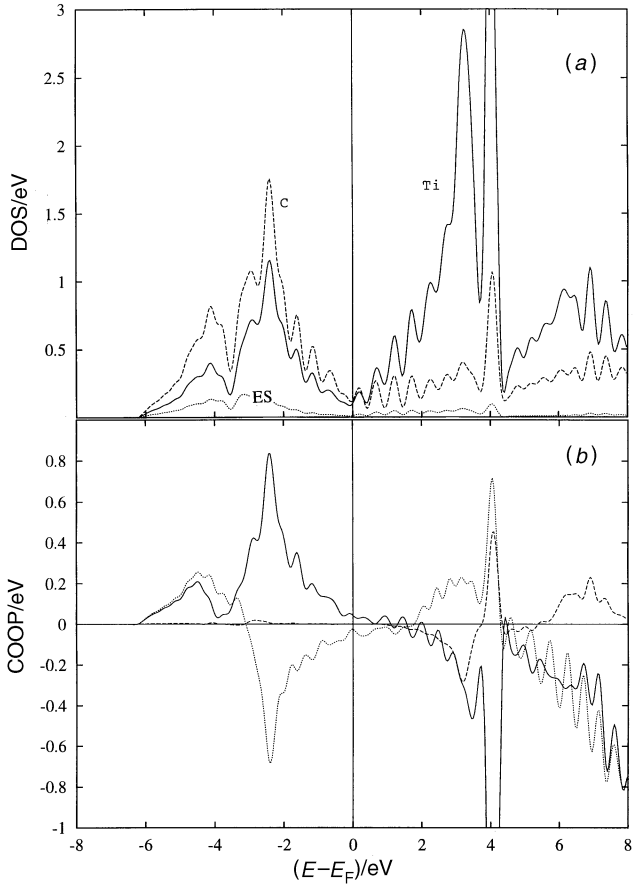

Fig. 5 TiC: (*a*) site projected densities of states (solid line Ti; dashed line C; dash-dotted line ES); (*b*) partial COOP for pair interactions: Ti–C (solid line), Ti–Ti (dashed line), C–C (dotted line)

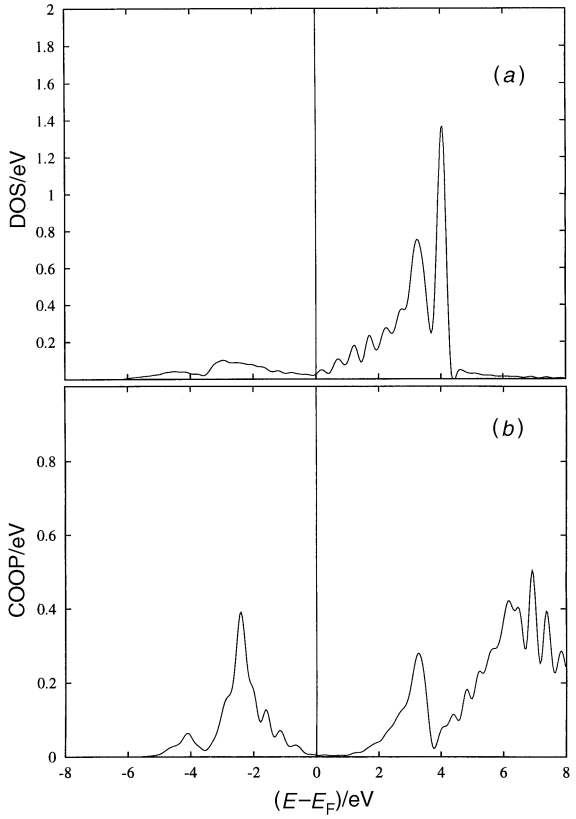

Fig. 6 O_h crystal-field decomposition of the Ti d-orbital DOS: (*a*) Ti $d(t_{2g})$; (*b*) Ti $d(e_g)$

This is explained more quantitatively by examining the COOP shown in the same energy window as the DOS in Fig. 5(*b*). They are resolved for three kinds of interactions in the lattice, namely Ti–C, Ti–Ti and C–C. The latter two types of interactions show fewer bonding features than the former; Ti–Ti interactions are clearly less predominant (for the reasons argued above) than C–C interactions, which exhibit bonding and antibonding states in the valence band whereas Ti–Ti bonding features can only be seen in the conduction band. Thus, in TiC 3d–2p bonding is the driving bonding force. Two types of 3d–2p bonding are found with increasing energy, *i.e.* pd_σ predominates over pd_π in the valence band, whence the directional character of the bonding in this compound. Since the former are stronger the antibonding counterparts are reversed, following energetical order: pd_π* resembled by the antibonding peak at 4 eV and pd_σ* at higher energies.

In our two carbide systems, the directionality of the bond is reduced by the presence of Al, which acts through its p and d states in its bonding to Ti. From this there is an increase in the amount of d character in the valence band. This is indicated by the larger occupation of Ti 3d with 0.52 and 0.47 electrons in Ti_2AlC and Ti_3AlC, respectively, in comparison to the Ti d-band occupation in TiC. As a matter of fact, it explains the larger $n(E_F)$ of the former and its vanishing value in TiC.

Discussion and Conclusion

Experimentally, it was found that Ti–C bonding was the driving force which controlled the C–TiAl and C–Ti_3Al interactions.[3] These experimental features agree rather well with the results of our calculations, indicating strong Ti–C interactions which are reminiscent of the formation of TiC in the

immediate vicinity of the carbon fibre. This should destabilize the actual alloy lattice, leading to the formation of precipitates.

Our investigation has shown that carbon plays different roles in Ti_2AlC and in Ti_3AlC. While it bonds mainly to Ti in the former, both Ti–C and Al–C bonds are present in the valence band for the latter. This is supported experimentally because the solubility of carbon is higher in Ti_3AlC when it enters the alloy lattice. Valence and conduction bands are largely separated by non-bonding states at E_F in Ti_3AlC, whereas bonding metallic Ti–Al interactions are present at E_F in Ti_2AlC. This could point to a higher 'ionic' character in Ti_3AlC and a higher 'metallic' character in Ti_2AlC.

Our comparison of the bonding within Ti_2AlC and Ti_3AlC to its characteristics in TiC shows that Al reduces the directionality of the bonding mainly through its p states, as well as its d ones which interact with Ti d states. From this there is an increase in the amount of d character in the valence band.

To conclude, the present study has brought a new insight into the bonding features in the C–Ti–Al ternary system, allowing for a more quantitative description on the chemical bonds.

Facilities provided by the computer centre of the Université Bordeaux 1 (CRIBx1) are acknowledged. Part of the calculations was performed within the MNI pole of intensive computations.

References

1 D. Vujic, Z. Li and S. H. Wang, *Metall. Trans. A*, 1988, **19**, 2445.
2 M. Morinaga, J. Saito, N. Yukawa and H. Adach, *Acta Metall. Mater*., 1990, **38**, 25.
3 L. Clochefert, PhD Thesis, Université Bordeaux 1, 1995.
4 S. R. Chubb, D. A. Papaconstantopoulos and B. M. Klein, *Phys. Rev. B*, 1988, **38**, 12120.
5 H. Erschbaumer, R. Podloucky, P. Rögl, G. Temnitschka and R. Wagner, *Intermetallics*, 1993, **1**, 99.
6 S. F. Matar and J. Etourneau, *J. Alloys Compd*., 1996, **233**, 112.
7 A. R. Williams, J. Kübler and C. D. Gelatt Jr., *Phys. Rev. B*, 1979, **19**, 6094.
8 U. von Barth and L. Hedin, *J. Phys. C*, 1972, **5**, 1629; J. F. Janak, *Solid State Commun*., 1978, **25**, 53.
9 R. Hoffmann, *Angew. Chem., Int. Ed. Engl*., 1987, **26**, 846.
10 V. Eyert and S. F. Matar, 1994, unpublished results.
11 W. B. Pearson, *Acta Crystallogr., Sect. A*, 1980, **36**, 724.
12 P. Blaha and K. Schwarz, *Int. J. Quantum Chem*., 1983, **23**, 1535.
13 J. Häglund, G. Grimvall, T. Jarlborg and A. Fernandez Guillermet, *Phys. Rev. B*, 1991, **43**, 14400.

Paper 6/05113H; *Received* 23*rd July* 1996